Two rods confined by positive plates: effective forces and charge distribution profiles

2006 J. Phys.: Condens. Matter 18 S2335

(http://iopscience.iop.org/0953-8984/18/36/S08)

INSTITUTE OF PHYSICS PUBLISHING JOURNAL OF PHYSICS: CONDENSED MATTER

J. Phys.: Condens. Matter **18** (2006) S2335–S2352 doi:10.1088/0953-8984/18/36/S08

Two rods confined by positive plates: effective forces and charge distribution profiles

G Odriozola, F Jiménez-Ángeles and M Lozada-Cassou

Programa de Ingeniería Molecular, Instituto Mexicano del Petróleo, Lázaro Cárdenas 152, 07730 México, DF, Mexico

Received 7 June 2006
Published 24 August 2006
Online at stacks.iop.org/JPhysCM/18/S2335

Abstract

The effect of confinement on the interaction force between two negatively charged rods is studied through Monte Carlo simulations. Confinement is produced by two parallel, charged or uncharged plates. The system is immersed in a 0.1 M 1–1 restricted primitive model electrolyte. The effect on the rod–rod effective force by the plate charge distribution is analysed. A strong modification of the rod–rod effective force due to confinement is found, as compared to the bulk case. In particular, rod–rod attraction was found for plates having a charge equal to that of fully charged bilipid bilayers. In spite of the simplicity of the model, these results agree with some DNA–phospholipid experimental observations. On the other hand, for a model having the plate charges fixed on a grid, very long range, oscillatory rod–rod effective forces were obtained.

(Some figures in this article are in colour only in the electronic version)

1. Introduction

In soft matter science, confinement is known to induce ordering, produce density fluctuations, provoke dielectric changes on liquids, affect diffusion processes, promote layering, enhance miscibility in polymer blends, and yield anomalous attractions between like charged colloidal particles [1–9]. This last effect was observed experimentally by accessing the pair correlation function by means of video microscopy and optical tweezers [10]. Additionally, biological set-ups such as those formed by plate-like charged lipid bilayers and rod-like DNA molecules show that, under certain conditions, confining bilayers induce a dense parallel 2D array of like charged DNA molecules [11–15]. Hence, it seems clear that there is a strong link between polyelectrolyte stacking and confinement.

The extensively used theory to explain interactions among charged colloidal particles is that of Derjaguin, Landau, Verwey, and Overbeek (DLVO) [16]. This is based on the Poisson–Boltzmann theory which deals with the electrostatic interaction among charged colloids and ions. This theory predicts that like charged colloids should repel each other following a screened Coulomb potential. There is, however, experimental evidence [17] and theoretical

proof [18] that under certain conditions two like charged macroparticles attract each other in bulk, and so this mean field theory cannot predict this unintuitive behaviour. On the other hand, there is also experimental evidence that like charged colloids, which do not attract in bulk, attract under confinement [10]. Theories based on the Poisson–Boltzmann equation cannot capture this peculiar behaviour, since they neglect many body correlations. On the other hand, to the best of our knowledge, there are no integral equations or density functional theoretical studies for the interaction between two macroparticles under confinement. Since they take into account many body correlations, these theories are expected to well describe the system behaviour. Finally, computer simulations, which had been successfully used for supporting theories, had not been employed for studying the effect of confinement on the interaction of two macroparticles.

Experiments of DNA plus phospholipids, in a low concentrated monovalent electrolyte solution, show self-assembling into lamellar structures, where DNA molecules are sandwiched between a stack of lipid bilayers. A transition from loose to compact 2D DNA ensembles has been found in these experiments by simply modulating the bilayer charge density. For low plate charge densities the loose 2D DNA structure occurs, whereas for higher charge densities the stack progressively compacts. Recently, we studied the effective interaction between two like charged parallel rods, which mimics two rod-like DNA molecules in an electrolyte solution [19]. We found that for a 0.1 M monovalent electrolyte rods repel each other. Additionally, attraction occurs when the like charged rods are in a highly enough concentrated electrolyte. The fact that DNA remains close in the presence of the highly charged confining plate-like lipid bilayers suggests that confinement may produce a similar effect as that of a concentrated electrolyte. This motivated us to study the influence of confinement on this particular two-rod system. This is done by means of Monte Carlo (MC) computer simulations. For that purpose, two like charged negative rods are considered, as in the previous work, and two positive charged plates are included mimicking the confining bilayers. Hence, different plate–plate distances and charge on plates are studied, for a 0.1 M 1–1 electrolyte. In addition, with the aim of elucidating the influence of the charge arrangement on plates, we considered three different models for the plate charge distribution.

The paper is structured as follows. Section 2 gives the computer simulation details. Results are presented in section 3, and section 4 summarizes the main contributions and tackles some conclusions. We have included an appendix to discuss the electrical field produced by the system under different conditions.

2. Simulations

Monte Carlo (MC) simulations were performed to study a system consisting of two infinitely large, parallel, negative rods confined by two parallel, positive plates of finite thickness. These hard macroparticles (rods and plates) are immersed in a 1–1 restricted primitive model (RPM) electrolyte. The simulation box has side lengths $L_x = L_z = 200$ Å, and $L_y = 125$ Å. The origin of coordinates is set at the box centre. Plates are located parallel and symmetric to the $z = 0$-plane, with a surface–surface separation distance τ. Rod axes are placed parallel to the y axis at $x = \pm(R + t/2)$, $z = 0$, with R being the rod radii and t the rod–rod minimal surface distance. The plate–rod surface distance is $h = (\tau - 2R)/2$. A schematic representation of the system is given in figure 1.

For simplicity, plates, rods, and solution have the same dielectric constant. RPM consists of hard spheres with a centred point charge, such that their electrostatic interaction is

$$U_E(r_{ij}) = \frac{\ell_B z_i z_j}{\beta r_{ij}}, \tag{1}$$

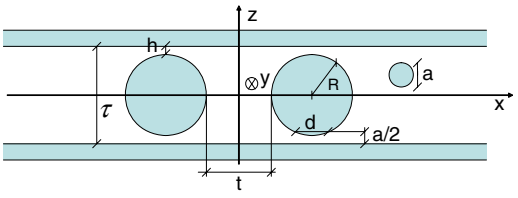

Figure 1. Schematic representation of the system.

with $\beta = 1/k_{\mathrm{B}}T$, k_{B} the Boltzmann constant, $T = 298$ K the absolute temperature, z_i and z_j the valences of sites i and j, $\ell_{\mathrm{B}} = \frac{\beta e^2}{\epsilon} = 7.14$ Å the Bjerrum length, $\epsilon = 78.5$ the dielectric constant, and r_{ij} the interparticle distance. The electrostatic interactions among macroparticles and between macroparticles and ions are also given by equation (1) with i and/or j running over the macroparticle sites.

We assigned to plates a charge density of $\sigma_0 = 0.229$ C m^{-2} ($+e$ per 70 Å^{-2}) for each surface, in correspondence with a fully charged cationic lipid membrane [20]. To study the effect of varying the plate charge density, for some systems we assigned a fraction of this charge, expressed as a percentage. Three ways of distributing the charge on plates were explored. The first consists of placing $+e$ charges in the centre of 5 Å hard spheres, which are confined within the plate surfaces, and are moved by following the MC criterion. The hardcore interaction of these 5 Å spheres is switched on just among themselves, i.e. their centres can approach the plate surfaces but cannot surpass them, and they do not interact with fluid ions. This model is named *confined spherical ions* (CSIs). The second way is by placing the $+e$ charges over triangular grids, which are frequently and randomly moved in the x and y directions to mimic a continuous charge distribution. These grids are placed on the surfaces of the plates. This model is named the *random triangular grid* (RTG). The third way is by placing the $+e$ charges over triangular grids, as in the previous case, but fixing them in these positions. This third model is named the *triangular grid* (TG). Rods have an $-e$ site every 1.7 Å, as do DNA molecules [20].

Rods have a radius of $R = 10.5$ Å, consistent with a hydrated DNA molecule. Plates are 5 Å thick to allow fluid–fluid correlations between the interplate and bulk sides of the plates [21]. These correlations are expected in real 40 Å thick bilayers, due to their low dielectric constant. We fixed the concentration of the 1–1 electrolyte to $\rho_{\mathrm{s}} = 0.1$ M, and assigned to ions a diameter of $a = 4.25$ Å.

Additional anions are added to make the system electroneutral. Periodical boundary conditions are set for all directions. The Ewald summation formalism is employed to deal with Coulomb interactions [22, 23]. To access all phase space volume, i.e. to allow for ion interchange between the confined and unconfined regions, movements having a large maximum displacement are made. Figure 2 shows a front view snapshot of an equilibrated system having $h = 0$, $t = a$, and a 100% of plate charge. Here, the plate charge was distributed by the first method, blue means negative and red positive, and sizes are scaled except the 5 Å plate charges, which are represented smaller.

Electrostatic contributions to the forces acting on the macroparticles (rods and plates) are obtained by

$$\mathbf{F}_{\mathrm{el}} = \left\langle \sum_i \sum_j \nabla U_E(r_{ij}) \right\rangle, \tag{2}$$

where i runs over the sites of the reference macroparticle and j runs over all other sites. The contact (depletion) contribution is obtained by integrating the ion contact density, $\rho(s = cte)$,

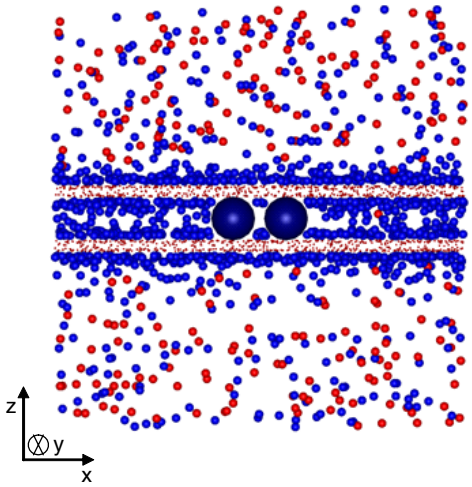

Figure 2. Snapshot of an equilibrium configuration of a system consisting of two rods sandwiched by two positive, confining plates. Conditions are electrolyte 1–1, $\rho_s = 0.1$ M, 100% charged CSI plates, $h = 0$, $t = a$. Positive charges are light grey (red), negative are dark grey (blue).

$$\mathbf{F}_c = -k_B T \int_s \rho(s = cte)\mathbf{n}\,\mathrm{d}s, \tag{3}$$

where s refers to the macroparticle surface of closest approach and $\mathbf{n}$ is a unit normal vector. These two contributions to the force are interdependent [19].

We should mention that the purpose of the model here employed is not to give detail about the very complex DNA–phospholipid interactions, but to bring out some interesting effects produced by confinement on the interaction of rods. Detailed DNA–DNA and DNA–phospholipid interactions can be modelled by considering all-atom or coarse-grained molecular models, which naturally account for the inhomogeneous dielectric constant of the medium, since it is explicitly included, solvent entropy driven effects produced by its ordering, and entropy driven effects associated with the conformation change of the bilayer membranes, among others. Hence, our results should be taken as an effort to understand confinement in real systems.

3. Results

As pointed out above, for all results here studied we fixed the rod radii to $R = 10.5$ Å, their charge to one $-e$ each 1.7 Å (corresponding to a surface charge density of 0.143 C m^{-2}), the plate thickness to 5 Å, the ion radii to $a = 4.25$ Å, and a 1–1 bulk electrolyte concentration of 0.1 M. This section is divided in four parts. As a reference, we first present the results for unconfined rods, i.e. two rods in bulk. Secondly, results for confinement produced by positively charged plates are given. Next, the influence of the plate charge distribution on the rod–rod interaction is discussed, and finally, results for confining plates with half and no positive charge are analysed.

3.1. Unconfined rods

In the absence of plates, the interaction pressure (effective forces per unit of rod area) between two rods in bulk is given in figure 3 as a function of the distance between rod surfaces, t. Note

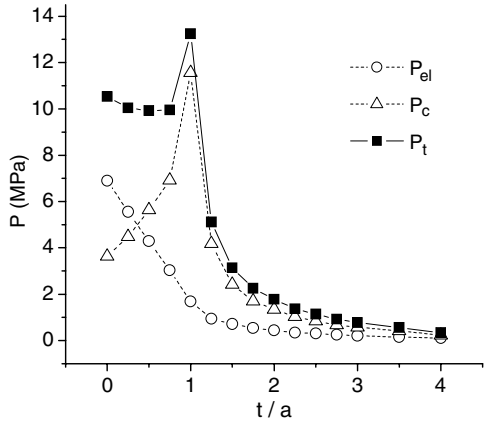

Figure 3. Electric (P_{el}), contact (P_c), and total (P_t) pressures as a function of t for two unconfined rods. Conditions are electrolyte 1–1, $\rho_s = 0.1$ M, $h \to \infty$ (no plates).

that system symmetry makes the rod–rod forces have only components different from zero on x. These components are

$$P_i = \frac{F_{ix}}{2\pi R L_y} \tag{4}$$

where i can be el or c, standing for electric or contact, respectively. The total pressure, P_t, results from the sum of these interdependent contributions. It is seen that both contributions are always repulsive as well as the net force. P_{el} being monotonically decreasing, since it is likely that charged rod inherent repulsion decays with distance and since more counter-ions interpose between them as t increase. When rod double layers become independent from each other, both contributions become zero, as expected. P_c, however, behaves differently. It increases with distance for $t < a$, and decays for $t < a$, showing a maximum for $t = a$. To understand this behaviour, one should pay attention to how the charge distribution profiles around the macroparticles, $\rho_{el}(x, z)$, change with t. This is defined by $\rho_{el}(x, z) = z_+ g_+(x, z; \tau, t) + z_- g_-(x, z; \tau, t)$, with $g_+(x, z; \tau, t)$ ($g_-(x, z; \tau, t)$) the cation (anion) distribution profiles, given τ and t. These profiles in turn are linked to the electric field maps given in the appendix. Figure 4 shows $\rho_{el}(x, z)$ for $t = 0, 0.75a$, $1.5a$, and $2.25a$. For $t < a$ (plots (a) and (b)) figure 4 shows large ρ_{el} values at $(x = 0, z = \pm\sqrt{R_a^2 - (R + t/2)^2})$, with $R_a = R + a/2$. This indicates the formation of two lines of counter-ions along the rod dumbbell. These counter-ions put pressure on both rods, producing strong repulsive P_c contributions, which are not compensated by the external counter-ions [19]. Hence, as t increases, the lines of counter-ions approach each other, producing larger contact force components on the x axis. This explains the increasing trend of P_c with t for $t < a$. For $t > a$, the peaks at $(x = \pm t/2, y = 0)$ decrease with t (figures 4(c) and (d)) and so does the contact contribution. This produces the maximum of P_c at $t = a$, as well as the maximum of P_t. Finally, the work per unit of charged site necessary to move the rods from $t = 4a$ to $t = 0$ is 2.13 $K_B T$/site.

3.2. Influence of confinement

Keeping all the same conditions fixed as in the previous subsection, we now study the influence of confinement by including plates in the system. As a first experiment, we consider the plates to be fully charged (100%), in contact with rods ($h = 0$), and having their charge distributed according to the CSI model (charge sites are confined by plate boundaries and are moved by following the MC criteria), which probably describes to some extent the distribution of phospholipid charged heads inside the bilayer (plates).

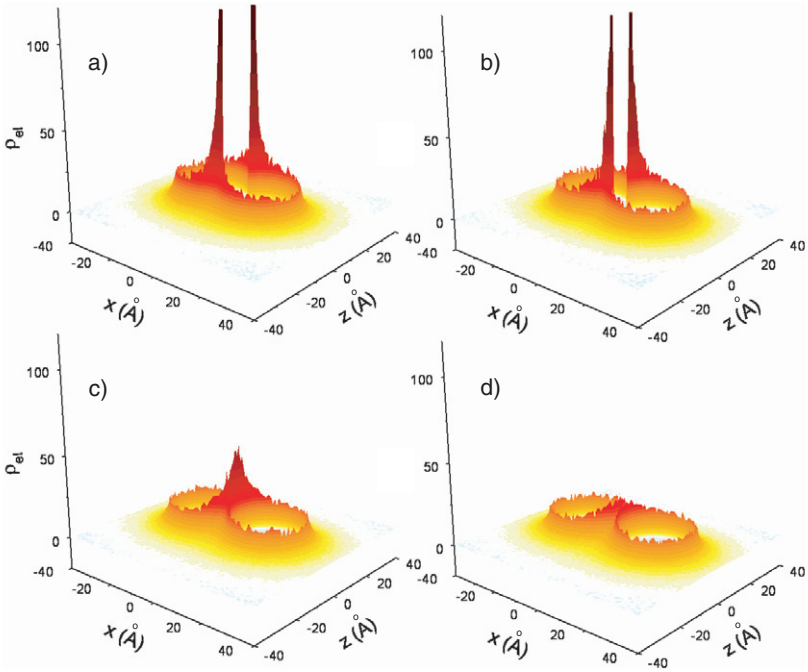

Figure 4. $\rho_{el}(x, z)$ for the following conditions: electrolyte 1–1, $\rho_s = 0.1$ M, and $h \to \infty$. (a)–(d) $t = 0, 0.75a$, $1.5a$, and $2.25a$, respectively. Darker tones indicate larger absolute values of $\rho_{el}(x, z)$, which is always positive in the four plots.

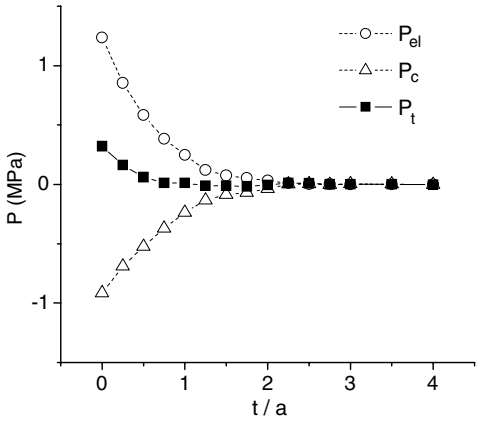

Figure 5. Electric (P_{el}), contact (P_c), and total (P_t) pressures as a function of t when highly charged confining plates are present and $h = 0$. Conditions are electrolyte 1–1, $\rho_s = 0.1$ M, 100% charged CSI plates, and $h = 0$.

The pressures obtained from this experiment are shown in figure 5. They strongly contrast with those shown in figure 3 in many aspects. First, the pressure is much smaller than for the unconfined case (compare the scales of both figures). Second, the range of the interaction is much smaller for the confined case. In particular, the total pressure is very small due to the counterbalance of a small repulsive P_{el} and a small attractive P_c. This leads to a work per

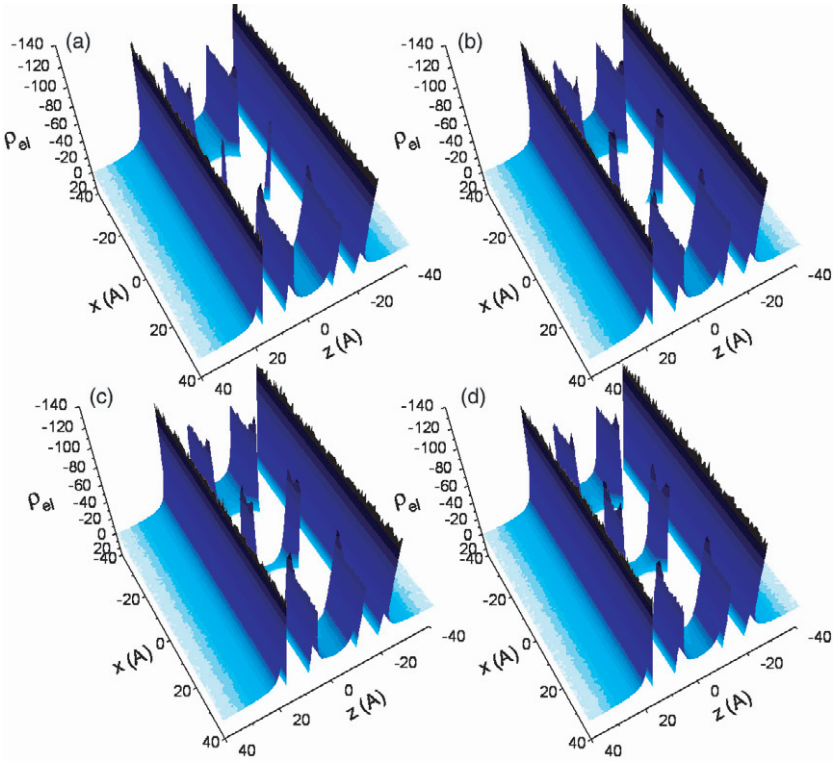

Figure 6. $\rho_{el}(x, z)$ for the following conditions: electrolyte 1–1, $\rho_s = 0.1$ M, 100% charged CSI plates, and $h = 0$. (a)–(d) $t = 0$, $0.75a$, $1.5a$, and $2.25a$, respectively. Darker tones indicate larger absolute values of $\rho_{el}(x, z)$, which is always negative in the four plots.

unit of charged site necessary to move the rods from $t = 4a$ to $t = 0$ of 0.01 K_BT/site (two orders of magnitude lower than the unconfined case). In addition, it is slightly attractive in the region $1.25a \leqslant t \leqslant 2a$, and clearly positive for $t \leqslant a$. In fact, we obtain a very small but negative work per unit of rod site necessary to move the rods from $t = 4a$ to $t = 1.25a$, i.e., -0.0005 K_BT/site. However, due to the intrinsic numerical error, we cannot guarantee this attraction.

These differences are explained by the strong change in the charge distribution profiles around the macroparticles. They are shown in figure 6 for $t = 0$, $0.75a$, $1.5a$, and $2.25a$. As can be seen, the charge density surrounding the rods, which is positive for the unconfined case, is now negative. It should be noted that this case corresponds to the one shown in figure 2, where just a single cation is seen in the confined region for this particular snapshot. Hence, cations are expelled out from the sandwiched region, in favour of anions, which are the plate counter-ions. This large anion concentration in the interplate region and outside the area in between rods counterbalances the rod–rod electrostatic repulsion by exerting an electrostatic external contribution, producing a remarkable decrease of P_{el}. On the other hand, the large cation peaks at $(x = 0, z = \pm\sqrt{R_a^2 - (R + t/2)^2})$, for the unconfined case, are not present any more, and hence P_c decreases, since these peaks were responsible for the large contact repulsive contribution. Moreover, the anion peaks that grow outside the rods and close to the plates in this case are higher than the anion peaks at $(x = 0, z = \pm\sqrt{R_a^2 - (R + t/2)^2})$, giving rise to an attractive P_c for $t \leqslant 0.75a$. These outside peaks are seen in figure 6 for all distances

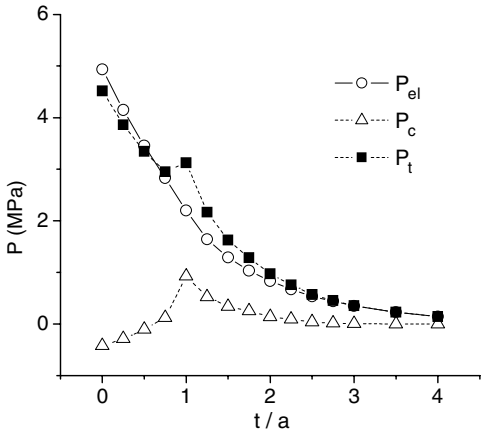

Figure 7. Electric (P_{el}), contact (P_c), and total (P_t) pressures as a function of t. Conditions are electrolyte 1–1, $\rho_s = 0.1$ M, 100% charged CSI plates, and $h = a$.

t. It is also seen that the inner peaks at $(x = 0, z = \pm\sqrt{R_a^2 - (R + t/2)^2})$ are smaller for figures 6(a) and (b) than for figures 6(c) and (d). In fact, figure 6(a) shows very narrow peaks at $(x = 0, z = \pm\sqrt{R_a^2 - (R + t/2)^2})$, indicating that anions can barely enter these inter-rod regions.

Figure 6 shows large interplate ionic depletion regions due to the presence of the rods. As expected, these depletion regions unbalance the contact forces inside and outside the plates, producing an attractive net contact force per unit of plate area of -6.72 MPa. This force is practically independent of t (the reported value is the average). The electric contribution to the pressure on plates is repulsive but small, i.e. 1.12 MPa. This leads to a total pressure of -5.6 MPa.

A second computer experiment was carried out for the same conditions but $h = a$. Resulting pressures are plotted in figure 7. They show a somewhat intermediate behaviour between cases $h = 0$ and $h \to \infty$ (compare figures 3 and 5 with figure 7). That is, both contributions, P_c and P_{el}, were diminished by confinement, but in this case the decrease is not as pronounced as for $h = 0$. Notice that the extent of the effective rod–rod interaction becomes much larger than for $h = 0$, and comparable with case $h \to \infty$. That is, a slight increment of the plate separation remarkably affects the extent of P_t. The work per unit of rod sites to move the rods from $4a$ to 0 becomes 0.78 $K_B T/site$, which lies in between the values obtained for $h \to \infty$ and $h = 0$. Additionally, other features such as the contact force peak at $t = a$ prevail, which is a signature of the presence of rod counter-ions in between the rods, as found for unconfined rods. Nevertheless, the negative contact contribution for short rod–rod distances indicates the presence of large anion peaks outside the rods, as found for $h = 0$.

These features are depicted in figure 8, where the charge density profile is shown for $t = 0$, $0.75a$, $1.5a$, and $2.25a$. The yellow regions close to the rods and at the midplane indicate the presence of rod counter-ions (cations). It is observed that they enter in between the rods as t increases. This is similar to case $h \to \infty$. Anion peaks outside the rods are larger than those in between them for $t = 0$ and $0.75a$ (figures 8(a) and (b)). An important difference with respect to case $h = 0$ is that interplate ionic depletion regions are smaller. This affects the contact plate–plate pressure, which in this case is -3.6 MPa. The electric contribution becomes attractive, i.e. is -1.0 MPa, and the total pressure is -4.6 MPa, for $t = 0$. In this case, the attractive pressure on plates decreases, with t reaching values close to -3 MPa for $t > 2a$.

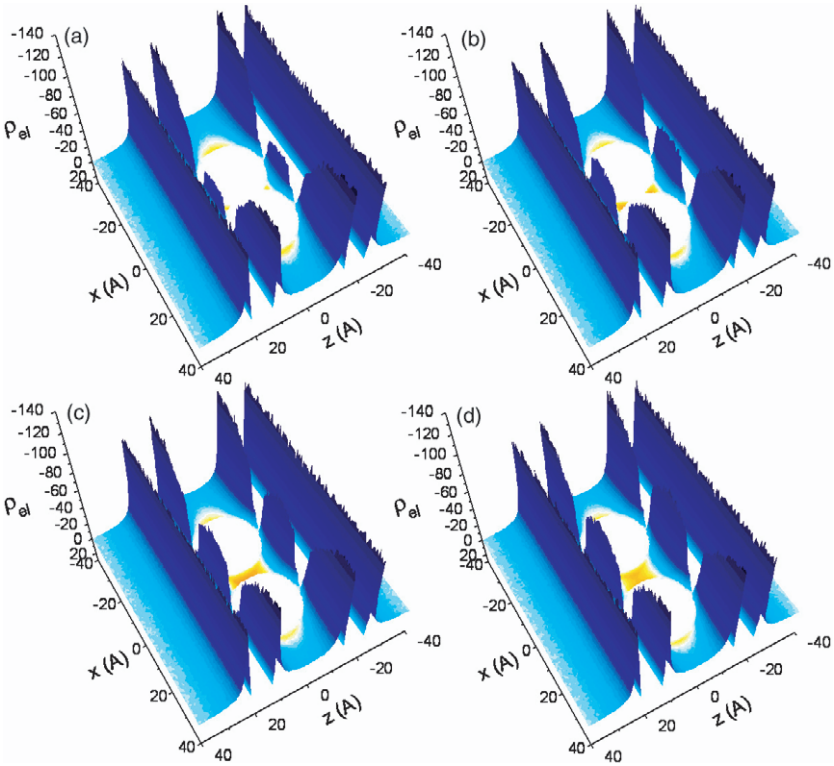

Figure 8. $\rho_{el}(x, z)$ for the following conditions: electrolyte 1–1, $\rho_s = 0.1$ M, 100% charged CSI plates, and $h = a$. (a)–(d) $t = 0$, $0.75a$, $1.5a$, and $2.25a$, respectively. Darker tones indicate larger absolute values of $\rho_{el}(x, z)$, while reddish colours mean positive and blueish negative. Positive values are only seen in between rods and at the outside of rods close to the midplane ($z = 0$).

3.3. Effect of the discrete charge of plates

So far we have shown that confinement strongly affects the interaction between two macroparticles (rods, in our case). In the present section, we study the influence of the different models for the plate charge distribution on the rod–rod effective pressure, i.e. models CSI, RTG, and TG introduced in section 2. For that purpose, we started by analysing the positive charge distribution inside the plates, $\rho_{el}^{in}(x, z)$, obtained for case $h = 0$, $t = 0$, and CSI. Here, $\rho_{el}^{in}(x, z)$ is defined by $z_+^{in} g_+^{in}(x, z; h, t)$, with z_+^{in} the valence and $g_+^{in}(x, z; h, t)$ the reduced concentration profile inside the plates, for given values of h and t. For these conditions, $\rho_{el}^{in}(x, z)$ is shown in figure 9(a), for the lowermost plate, where the rods are schematized for clarity.

It can be seen that, driven by energy and entropy, the plate charges move toward the plate surfaces, forming almost homogeneous distributed surface charge densities. This produces a practically null electric field inside plates (see the appendix). We recall that we are modelling positive phospholipids with an assumed head diameter of 5 Å. These surface charge densities are practically not influenced by the rod positions. This is maybe the most important conclusion, since it makes us think that a homogeneous surface charge distribution may also be appropriate to model this system. On the other hand, it is also true that a small deviation from a homogeneous surface charge distribution is observed. That is, charge peaks close to the rods are observed, which in turn produce relative depletion regions at their sides (valleys). These features are highlighted in figure 9(a), and easily observed in figure 9(b).

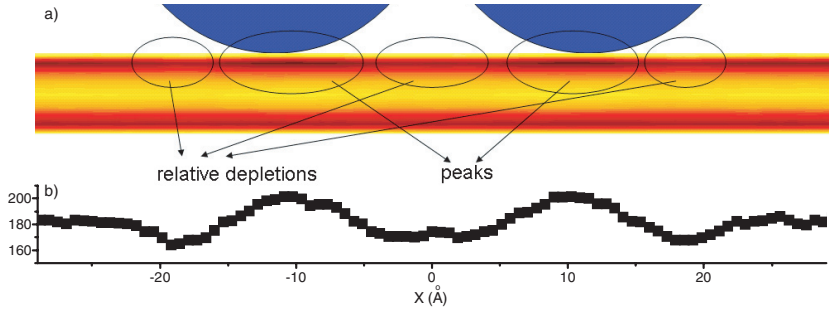

Figure 9. (a) $\rho_{el}^{in}(x, z)$ for planes. Darker tones indicate larger absolute values of $\rho_{el}^{in}(x, z)$. (b) $\rho_{el}^{in}(x, z = -11.5\ \text{Å})$. Peaks and valleys highlighted in (a) are easily seen in this plot. Conditions are electrolyte 1–1, $\rho_s = 0.1$ M, 100% charged CSI plates, $h = 0$, and $t = 0.25a$.

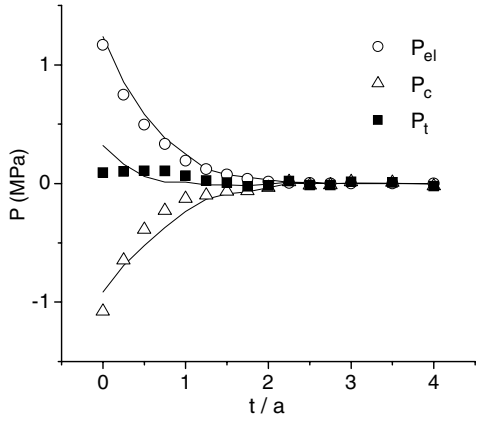

Figure 10. Electric (P_{el}), contact (P_c), and total (P_t) pressures as a function of t. Conditions are electrolyte 1–1, $\rho_s = 0.1$ M, 100% charged RTG plates, and $h = 0$. Lines correspond to the results presented in figure 5 (equal conditions but for CSI plates).

With this result in mind, let us test a simpler model where the positive charge on plates is distributed on triangular grids at both sides of each plate, which are independently, frequently, and randomly moved in the x and y directions, to mimic homogeneous surface charge distributions. This model was named the random triangular grid (RTG). The pressures on rods obtained by using RTG are presented in figure 10 and compared with those obtained from CSI. In general, a very similar behaviour is obtained for RTG and CSI. That is, in both cases, P_c are negative, monotonically increasing functions of t, yielding zero for $t > 2.5a$, and both P_{el} are positive, ever-decreasing functions of t, giving zero for $t > 2.5a$. Both models yield very small values of P_t for all t, being positive for $t < a$ and negative for $1.25a < t < 2.25a$. The main difference between RTG and CSI is the smaller value of P_t at $t = 0$ obtained for RTG. On the other hand, the obtained value of the total plate–plate force is -5.5 MPa, which is similar to that for the CSI model (-5.6 MPa). *From this comparison, we may conclude that the discrete nature of the bilayer charge does not strongly affect the forces on rods.* However, we wish to point out that for a lower charge density of the plates, there appear somewhat more important differences between the CSI and RTG rod–rod pressures at small plate–plate distances.

Leaving aside the small differences between the previous models, we still would like to know whether a structured fixed grid (FG) of discrete surface charge affects the rod–rod effective interaction. This, of course, is not expected to be a good model for a lipid bilayer, but may model a certain type of nanostructured material. Results are shown in figure 11. For $t \leqslant 0.5a$, they are qualitatively similar to those shown in figure 10, i.e. there is an attractive

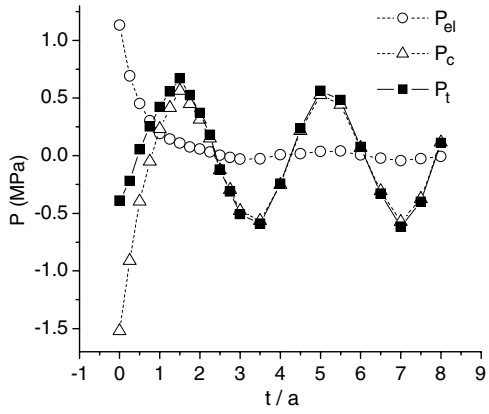

Figure 11. Electric (P_{el}), contact (P_c), and total (P_t) pressures as a function of t for a continuously like surface charge distribution on plates. Conditions are electrolyte 1–1, $\rho_s = 0.1$ M, 100% charged TG plates, and $h = 0$.

increasing P_c and a repulsive decaying P_{el}. For $t > 0.5a$, however, P_c yields positive values, reaching a maximum at $t = 1.25a$. Moreover, it periodically produces positive maxima and negative minima every $3.68a$, showing an oscillatory behaviour. These maxima and minima show similar absolute values, independently of t, in other words, this behaviour is very long ranged. Such behaviour strongly differs from the previous studied cases (RTG and CSI models), so that it is a consequence of the rod–plate interaction. On the other hand, P_{el} also shows an oscillatory behaviour, once the rods are far enough from each other, having an amplitude much smaller than that of P_c. Both P_{el} and P_c are in phase.

The charge distribution profiles are shown in figure 12 for the TG model, $t = 0$, $0.75a$, $1.5a$, and $3a$. In all plots of figure 12 peaks and valleys of the charge distribution appear close to plates. Naturally, peaks coincide with the locations of the positive charge on plates and valleys are between peaks. Hence, the peak to peak distance is equal to the x distance between adjacent charged plate sites; i.e., $\lambda = 7.8$ Å ($1.84a$). As shown in the appendix, the electric field clearly diverges from these charged sites on plates. By construction, the x and y positions of the internal charged sites of both plates are the same. Consequently, internal peaks and valleys of the charge distribution profile of one plate face those of the other. This produces a reinforcement of the effects that peaks and valleys produce on the rod effective forces. For instance, in figure 12(a) it is observed that the rod inner surfaces coincide with the valleys of $\rho_{el}(x, z)$, whereas the outside surfaces with peaks, explaining the attractive P_c at $t = 0$. In figure 12(b), the inner and outer rod surfaces do not match either peaks or valleys, and hence P_c is close to zero ($t = 0.75a$). For $t = 1.5a$, a maximum is observed for P_c, which is explained by the ionic peaks at contact with the inner rod surfaces (see figure 12(c)), and the valleys at contact with the external rod surfaces. The opposite situation is found for $t = 3a$, where peaks coincide with the outer rod surfaces whereas valleys with the inner surfaces (see figure 12(d)). *Hence, it becomes clear that this apparent long range rod–rod interaction is nothing but a periodical rod–plate double layer coupling effect.* Indeed, the P_c period of $3.68a$ is equal to 2λ, which is simply a consequence of the fact that an increment Δt of the relative rod positions implies a displacement of $\Delta t/2$ for each rod.

It must be noted that the behaviour of P_c depends on the ratio between the distance $d = 2\sqrt{(R + a/2)^2 - (R - a/2)^2} = 2\sqrt{2aR}$ (for case $h = 0$) and λ (see figure 1), and on the relative position between the charged sites of one plate and the other. For instance, if the

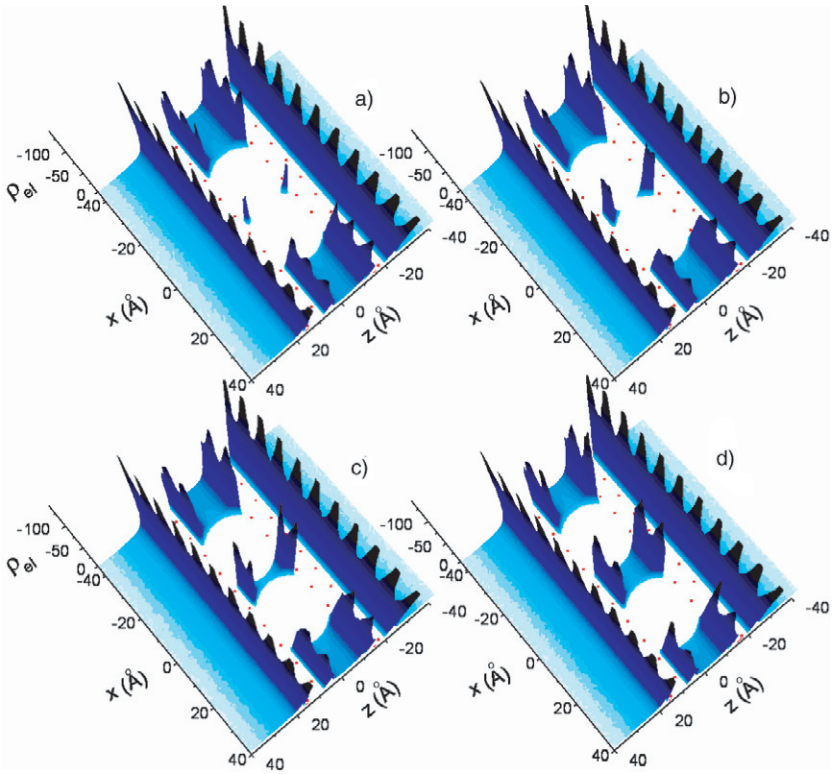

Figure 12. $\rho_{el}(x, z)$ for the following conditions: electrolyte 1–1, $\rho_s = 0.1$ M, 100% charged RTG plates, and $h = 0$. (a)–(d) $t = 0$, $0.75a$, $1.5a$, and $3a$, respectively. Darker tones indicate larger absolute values of $\rho_{el}(x, z)$. Dots in plates indicate where the discrete positive charge is located.

charged sites of the plates are placed out of phase by $\lambda/2$, P_c becomes a negative monotonically increasing function of t. The same happens for $\sqrt{2aR}/\lambda = (n + 1)/2$, with $n = 0, 1, 2, 3, \ldots$. In contrast, the oscillatory behaviour is strong when charged sites on plates are in phase and when $\sqrt{2aR}/\lambda = (n + 1/2)/2$. In this calculation $\sqrt{2aR}/\lambda = 1.21$ and the charged sites of one plate face the charged sites of the other, and this is why the oscillatory behaviour is clearly seen (in this case, $n = 2$). Another point to note is that the phase of the charges on the plates controls the phase of the charge induced in the electrolyte around the plates (see figure 12), which in turn rules the apparent rod–rod long range interaction. Hence, by changing the plate relative positions the rod–rod interaction minima change accordingly. This property may be of practical interest for nanostructure manipulation. Finally, we would like to add that the oscillatory behaviour of P_c should disappear for $h > a$.

3.4. Influence of plate charge density

DNA–lipid bilayer lamellar phase ensembles show a transition from condensed to loose DNA 2D arrays, modulated by the rate of cationic (di-oleoyl trimethylammonium propane) to neutral (di-oleoyl phosphatidylcholine) lipid molecules, which compose the confining bilayers. Experiments show that for a fully charged membrane, i.e. no neutral lipid added, DNA forms a condensed arrangement which has a DNA–DNA distance of 24.5 Å. This distance enlarges

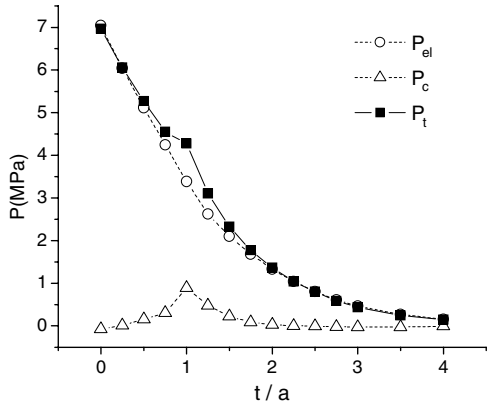

Figure 13. Electric (P_{el}), contact (P_c), and total (P_t) pressures as a function of h for plates having a 50% charge density. Conditions are electrolyte 1–1, $\rho_s = 0.1$ M, 50% charged RTG plates, and $h = 0$.

to 57.1 Å for 57% of the full charge density. Hence, this motivated us to study the effect of a smaller plate charge density on the rod–rod effective interaction.

Results for half the full charge density of plates are shown in figure 13. It is seen that P_t is a positive monotonically decreasing function of t. The work per unit of rod site to bring them in touch is 1.15 K_BT/site. Therefore, these results are consistent with the larger DNA–DNA distances found when neutral lipid is added to the bilayer. It should be noted that all pressure components of figure 13 are quantitatively and qualitatively similar to those shown in figure 7. Hence, a decrease of the surface charge density of plates has a similar effect to enlarging h. On the other hand, the pressure on plates is -5.1 MPa for $t = 0$, and decreases its absolute value to -4.5 MPa for larger t. In this case, the electric component is the larger contribution, being -4.8 at $t = 0$, and decreases to yield -3.2 for $t = 4a$.

The corresponding charge densities are shown in figure 14. As expected, much lower values of the charge density at contact with the plate surfaces are obtained, as a consequence of the lower charge of the plates. Hence, the interplate region becomes less crowded with anions (plate counter-ions) and positive charge densities are observed close to the rod surfaces. In particular, cations are allowed to fill the inter-rod regions at $(x = 0, z = \pm\sqrt{R_a^2 - (R + t/2)^2})$, which are responsible for the characteristic peak of P_c at $t = a$ (similar to figures 3 and 7). *Another consequence of a less crowded anionic interplate is the increment of the rod–rod effective repulsion*. That is, the fewer plate counter-ions there are in the interplate, the less compensated the inherent rod–rod repulsion becomes. Finally, notice that the charge density at contact with the outer plate surfaces becomes clearly dependent on the x coordinate. Since in this case the charge density on plates does not overcompensate that on rods, the charge distribution of the plate outside regions is strongly correlated with the presence of the rods.

When confinement is produced by uncharged plates the rod–rod total effective pressure becomes very repulsive, mainly due to the increase of the contact contribution. This is clearly seen in figure 15, where the large peak of P_c at $t = a$ makes P_t reach values close to 20 MPa. The general trend of the contributions is, however, similar to that already shown for unconfined conditions. In addition, the obtained pressure for plates is 2.4 MPa for $t = 0$, which decreases with t, yielding 0.4 MPa for $t = 4a$. Obviously, the plate total pressure is simply the contact contribution, since there is no electric component. Due to the fact of obtaining large positive plate–plate pressures, a configuration where rods are squeezed by plates is, in this case, not expected.

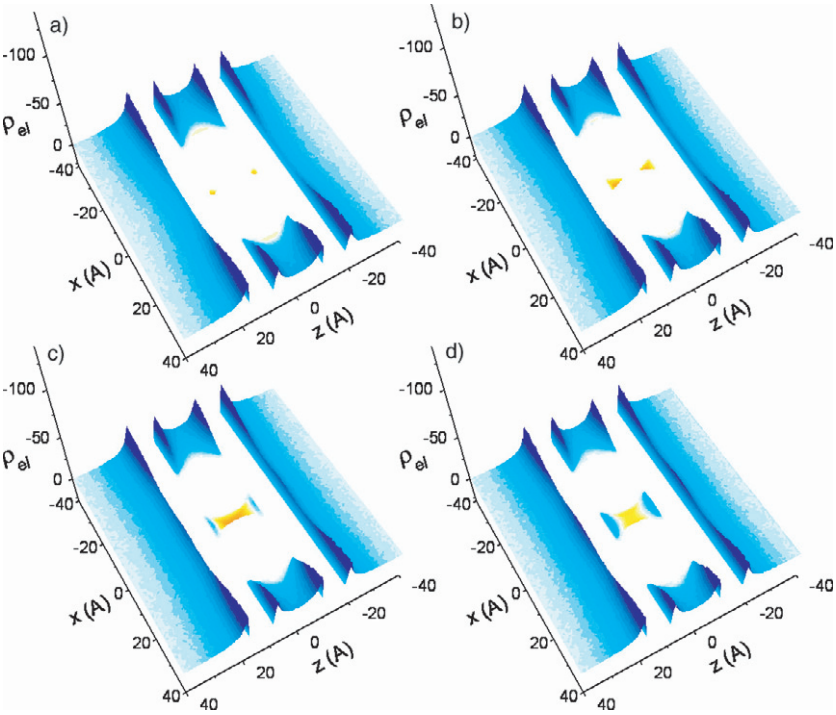

Figure 14. $\rho_{el}(x, z)$ for the following conditions: electrolyte 1–1, $\rho_s = 0.1$ M, 50% charged RTG plates, and $h = 0$. ((a)–(d)) Correspond to $t = 0$, $0.75a$, $1.5a$, and $2.25a$, respectively. Darker tones indicate larger absolute values of $\rho_{el}(x, z)$, while reddish colours mean positive and blueish negative. Positive values are only seen in between rods and at the outside of rods close to the midplane ($z = 0$).

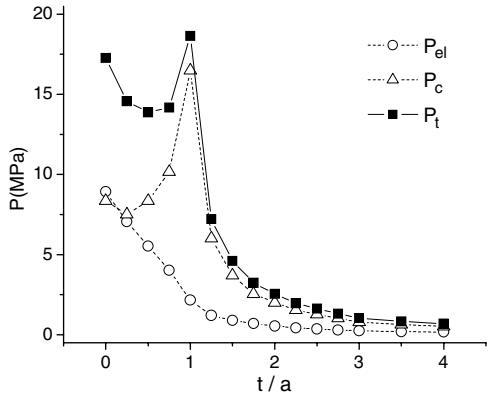

Figure 15. Electric (P_{el}), contact (P_c), and total (P_t) pressures as a function of t for uncharged plates. Conditions are electrolyte 1–1, $\rho_s = 0.1$ M, uncharged plates, and $h = 0$.

Confinement by uncharged plates also affects the charge distribution profiles. The fact that no ions can access part of the rod surfaces due to the presence of plates makes the system react by pushing more ions toward the accessible surfaces. In particular, the pore-like regions (large surface/volume rate), such as those located at $(x = 0, z = \pm\sqrt{R_a^2 - (R + t/2)^2})$, become crowded by cations (rod counter-ions), as shown in figure 16. Again, these cations exert large repulsive contact contributions on rods, explaining the huge effective pressure peak at $t = a$.

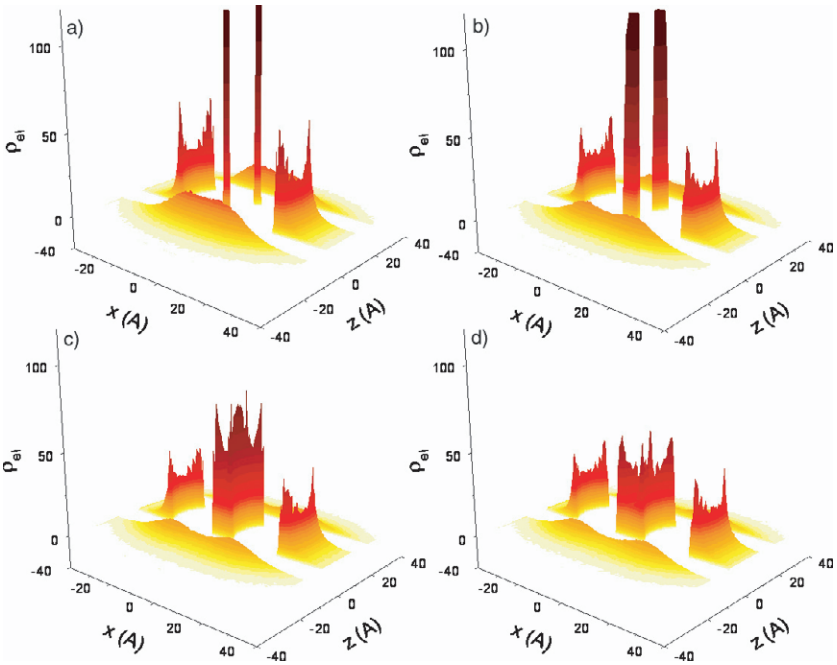

Figure 16. $\rho_{el}(x, z)$ for the following conditions: electrolyte 1–1, $\rho_s = 0.1$ M, uncharged plates, and $h = 0$. (a)–(d) $t = 0, 0.75a, 1.5a$, and $2.25a$, respectively. Darker tones indicate larger absolute values of $\rho_{el}(x, z)$, which is always positive in the four plots.

Another contribution to this pressure may be attributed to the correlation of ions located on the outside of the plates with the confined fluid; i.e., these ions were close to the rods for bulk conditions and now are forced to be farther from them, producing a less screened rod charge.

4. Conclusions

Monte Carlo simulations were performed to study a system counting on two charged, parallel rods, and two confining charged, parallel plates. The system is immersed in a 1–1 restricted primitive model electrolyte. Effective pressures acting on the macroparticles and the corresponding charge density profiles were calculated for different confinement conditions, i.e. the influence of the amount of charge of the confining plates, its distribution, and the plate–rod distance were studied. Compared with the absence of confinement, an enhancement of the inherent repulsive rod–rod effective force occurs in the presence of confining uncharged plates, whereas their repulsion systematically decreases by increasing the amount of positive charge on plates. Some cases even show attraction, as found for highly charged confining plates. Hence, highly charged plates promote a crowded stack of rods, and lower charged plates induce larger rod–rod separation distances. In spite of the roughness of the model here employed and its obvious limitations, these results agree with the observations of DNA confined by bilipid charged membranes. This suggests that most relevant effects are accounted for.

We considered three different models for the charge distribution on plates. We found that models having movable charged sites on plates (CSI model) and homogeneously like charged surfaces (RTG model) lead to similar results. On the other hand, a model having discrete, fixed site charges on plates, located forming a regular grid (TG model), induces a

very long range rod–rod effective interaction. This long range interaction shows an oscillatory behaviour, having maxima and minima periodically separated. As pointed out in the paper, it is a consequence of the double layer coupling between rods and plates. Since confinement rules the rod–rod force and since this interaction depends on the plate charge density, charge discreteness, and separation, these parameters could be useful for the construction of self-assembled systems.

In brief, it was shown that confinement and self-assembling are strongly connected, since attraction between rods and plates depends on a delicate balance between charge and excluded volume of all particles of the system. Additionally, self-assembling is linked to several interesting phenomena such as double layer coupling, counter-ion release, local violations of electroneutrality, and the appearance of ionic depletion regions. Our belief is that neither of them by itself rules self-assembling, but self-assembling involves all of them acting interdependently, as a whole.

Appendix. Electric field

We find it instructive to show what the electric field looks like for some of the cases studied here. We restrict ourselves to showing the $t = 0$ configurations, which correspond to figures 4(a), 6(a), 8(a), 12(a), 14(a), and 16(a). The electric field at a given xy position was calculated by simply averaging the electric force per unit of charge for all configurations. For obtaining the electric field for those xy positions that charged sites cannot access, a test point charge is included for the calculation. Naturally, this point charge is not accounted for during the simulation.

The obtained electric fields are shown in figure A.1. Figure A.1(a) corresponds to the unconfined case. There, it is seen that the electric field converges towards both rod axes, as expected. For the region outside the rods the electric field strength decays with the distance to the rod axes, whereas for the region between rods it points perpendicularly towards the $z = 0$ plane. In particular, there is a point of zero electric field at $(x = 0, z = 0)$, which is noted as lighter tones of the surrounding arrows.

The electric field is very disturbed by the presence of the confining plates, whether they are charged or not. When the plates are not charged, the disturbance of the electric field is due to charge correlations [18] through the plates with the fluid outside. This is in general seen in the following figures A.1(b) to A.1(f). Figure A.1(b), the CSI model with fully charged plates and $h = 0$, shows that inside the plates the electric field is very wek, due to the fact that the plate's charge is mostly located at the interface, as commented in section 3. This fact makes it difficult to obtain accurate values for this region, and this is why noise appears in the arrow directions. The diverging field from plates and the converging trend of field towards the rod axes reinforce and produce a very intense local electric field in between rods and plates. There also appear two regions of zero electric field at $z = 0$, outside the rods. Notice that the presence of the rods barely affects the electric field outside the interplate region. Recall that small positive (repulsive) values for the electric component of the force acting on plates were obtained under these conditions. This is consistent with the fact that the electric field diverging from plates outwards is slightly stronger than that diverging toward the midplane (this cannot be appreciated in the figure), and hence the charged sites on the outer plate surfaces experience larger forces than those at the inner surfaces.

For $h = a$, the CSI model, and fully charged plates (case A.1(c)), it is seen that the electric field inside plates increases with respect to the previous case. As mentioned in section 3, forces on plates are negative, i.e. attractive. A close inspection of the data reveals that the electric field diverging from plates toward the midplane is stronger than that diverging outwards from

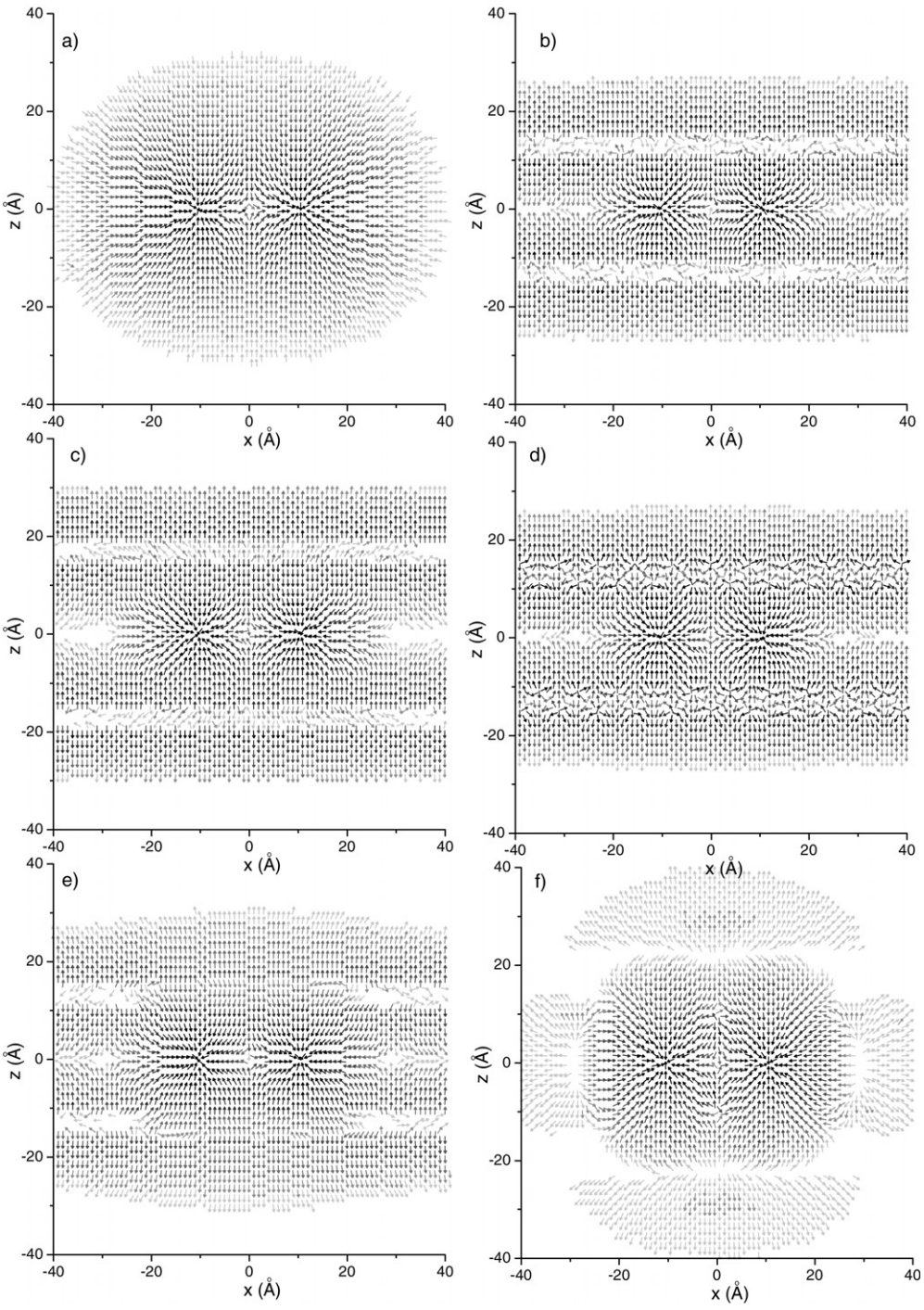

Figure A.1. Electric field for the different cases presented along the paper. Arrows indicate the field direction and darker tones points to larger absolute values of it. Tone changes are proportional to $\log(|\mathbf{E}|)$.

the plates (not appreciated in the figure). Additionally, from data analysis it becomes clear that the diverging electric field from plates is stronger close to the rods than farther away from them. This means that the electric component of the plate pressure is concentrated close to rods, suggesting that plates are supporting perpendicular shear stress. Hence, soft plates, such as bilipid membranes, would deform to surround rods, as shown experimentally for certain ADN–phospholipid complexes.

Figure A.1(d) corresponds to model TG. These charged sites are clearly distinguished in figure A.1(d) since they act as divergent sources of electric field. This, in turn, produces the interplate charge density peaks and valleys already shown in figure 12.

Figures A.1(e) and(f) show the results for plates charged with 50% of the full charge, and uncharged plates, respectively. Figure (e) shows that the electric field inside the plates points toward the inter-rod region, and that arrows that diverge from plates toward the plate midplane are darker than those pointing toward the opposite direction. This fact also well agrees with the attractive electric contribution for the pressure acting on plates, as mentioned in section 3. Again, this case suggests that shear stress is being supported by plates, since the electric field is stronger in the region close to rods. On the other hand, figure A.1(f) shows that the electric field diverges from some space regions which concentrate positive ions. For instance, divergences are seen at $(x = 0, z \cong \pm\sqrt{R_a^2 - (R + t/2)^2})$, at $(x \cong \pm 25$ Å, $z = 0)$, and at $z \cong \pm 22$ Å. These regions show positive charge distributions, as clearly shown in figure 16.

Finally, at lower charge densities one sees a larger polarization of the electrical field, which in turn indicates a higher correlation of the fluid inside and outside. This is due to the lower concentration of the electrolyte in between the plates, which, of course, underscreens the plate and rod charge less than in the high density case (see figure A.1(b)). An analysis of the electrical field of this system shows the formation of multipolar structures, which, according to the discussion given in the text, indicates that a loose assembly of rods would be favoured.

References

[1] Israelachvili J N 1992 *Intermolecular and Surface Forces* 2nd edn (New York: Academic)
[2] Lozada-Cassou M 1992 *Fundamentals of Inhomogeneous Fluids* ed D Henderson (New York: Dekker) chapter 8, pp 303–61
[3] Lozada-Cassou M and Henderson D 1986 *J. Colloid Interface Sci.* **114** 180
[4] Israelachvili J and Gourdon D 2001 *Science* **292** 867
[5] Levinger N E 2002 *Science* **298** 1722
[6] Zhu S *et al* 1999 *Nature* **400** 49
[7] Lozada-Cassou M, Olivares W and Sulbarán B 1996 *Phys. Rev.* E **53** 522
[8] Duda Y, Henderson D, Trokhymchuk A and Wasan D 1999 *J. Phys. Chem.* B **103** 7495
[9] Odriozola G, Aguilar F and López-Lemus J 2004 *J. Chem. Phys.* **121** 4266
[10] Han Y and Grier D G 2003 *Phys. Rev. Lett.* **91** 038302
[11] Rädler J O, Koltover I, Salditt T and Safinya C R 1997 *Science* **275** 810
[12] Wagner K *et al* 2000 *Langmuir* **16** 303
[13] Safinya C R 2001 *Curr. Opin. Struct. Biol.* **11** 440
[14] Wu C M *et al* 2004 *Macromolecules* **37** 4974
[15] Liang H, Angelini T E, Braun P V and Wong G C L 2004 *J. Am. Chem. Soc.* **126** 14157
[16] Russel W B, Saville D A and Showalter W R 1989 *Colloidal Dispersions* (Cambridge: Cambridge University Press)
[17] Kepler G M and Fraden S 1994 *Phys. Rev. Lett.* **73** 356
[18] Yu Y, Degrève L and Lozada-Cassou M 1997 *Phys. Rev. Lett.* **79** 3656
[19] Jiménez-Ángeles F, Odriozola G and Lozada-Cassou M 2006 *J. Chem. Phys.* **124** 134902
[20] Gelbart W M, Bruinsma R F, Pincus P A and Parsegian V A 2000 *Phys. Today* **53** 38
[21] Lozada-Cassou M and Yu Y 1996 *Phys. Rev. Lett.* **77** 4019
[22] Odriozola G and Guevara F 2004 *Langmuir* **20** 2010
[23] Alejandre J, Tildesley D J and Chapela G A 1994 *J. Chem. Phys.* **102** 4574